Metrol. Meas. Syst., Vol. XXI (2014), No. 2, pp. 233–246.

PAN POLSKA AKADEMIA NAUK

METROLOGY AND MEASUREMENT SYSTEMS

Index 330930, ISSN 0860-8229

www.metrology.pg.gda.pl

M&MS

EVALUATION OF DIFFERENT PROBING SYSTEMS USED IN ARTICULATED ARM COORDINATE MEASURING MACHINES

Agustín Brau, Margarita Valenzuela, Jorge Santolaria, Juan José Aguilar

I3A, University of Zaragoza, Maria de Luna 3, E-50018 Zaragoza, Spain (✉ agusba2003@gmail.com)

Abstract

This paper presents a comparison of different techniques to capture nominal data for its use in later verification and kinematic parameter identification procedures for articulated arm coordinate measuring machines (AACMM). By using four different probing systems (passive spherical probe, active spherical probe, self-centering passive probe and self-centering active probe) the accuracy and repeatability of captured points has been evaluated by comparing these points to nominal points materialized by a ball-bar gauge distributed in several positions of the measurement volume. Then, by comparing these systems it is possible to characterize the influence of the force over the final results for each of the gauge and probing system configurations. The results with each of the systems studied show the advantages and original accuracy obtained by active probes, and thus their suitability in verification (active probes) and kinematic parameter identification (self-centering active probes) procedures.

Keywords: articulated arm coordinate measuring machine, probing systems, self-centering active probe.

1. Introduction

Due to the increased utilization of AACMMs in the automotive, aerospace, railroad and energy industries, faster and more reliable calibration and kinematic parameter identification procedures are constantly sought [1–3]. A key aspect in this kind of procedures is the process of capturing data [4–11]. This data will be compared to nominal distance and position data obtained from a gauge or some other measurement instrument which functions as a gauge, thus allowing to define an error objective function to be minimized by means of a mathematical optimization procedure [7, 12–17].

Once the parameters have been identified, the best attainable accuracy in this type of equipment will greatly depend on the type and number of positions captured by the AACMM or robot arm [18, 19] and, ultimately, on the extent to which the number of influences on the capture of points can be minimized. Because the AACMM is a manually-operated instrument, the results obtained in its verification tests are subject to influences from the operator, mainly materialized through different probing forces during the data capture process. These external probing forces cause deformations to the gauge or to the probe [20, 21] which can result in the loss of accuracy in the verification procedure or during the process of capturing data for parameter identification.

In this work we present a comparison of the accuracy and repeatability obtained by four different probing systems (passive spherical probe, active spherical probe, self-centering passive probe and self-centering active probe), considering that passive probes are the ones that are dependent only on operators manual capture while active ones are able to automatically recognize the contact with the measuring object. In addition, the influence of the probing force over the self-centering passive probe measurements is analyzed through

Article history: received on Mar. 20, 2013; accepted on Dec. 03, 2013; available online on May. 15, 2014; DOI: 10.2478/mms-2014-0020.

its components in each of the axis-directions of the sixth reference system of the measurement arm, showing the advantages of the self-centering active probe in both calibration and kinematic parameter identification procedures.

2. Methodology

In order to capture the data a ball bar gauge was used to materialize nominal points and distances in the workspace of an AACMM. The ASME B89.4.22-2004 standard [22], the only existing standard in the field of AACMM verification, establishes verification procedures based solely on the capture of points through passive and active spherical tip probes. In this case, the influence of the probing force over the behavior of the articulated arm has been analyzed, obtaining the measurement error from the same physical points of the ball bar gauge through four different probing systems: passive spherical probe, active spherical probe, self-centering passive probe based on inverse kinematic coupling [7] and self-centering active probe based on parallel kinematics [23] (Fig. 1). In Fig. 1, the photos in the first row show the passive spherical probe (left) and active spherical probe (right) and those in the second row correspond to the self-centering passive probe (left) and self-centering active probe (right).

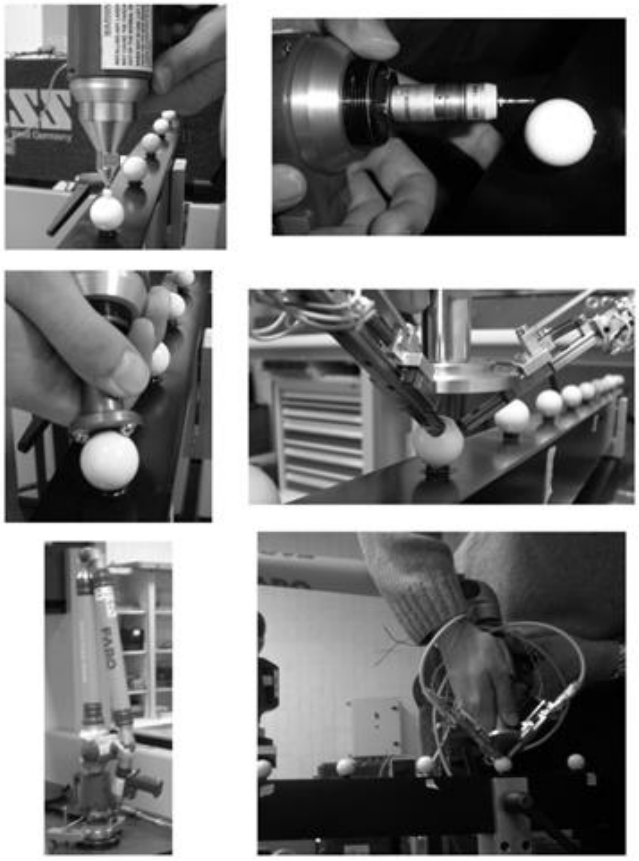

Fig. 1. Evaluated AACMM probing systems.

In the process of probing the points, a total of 28 spheres have been probed corresponding to seven different positions of the gauge in a quadrant of the AACMM workspace. From captured data we have analyzed the combined influence of the probing force and the probing direction in the final results with each probing system according to the gauge configuration.

3. Data capture setup

There are two ways to express the configuration of an AACMM as a function of the degrees of freedom of its articulations. The first one is to indicate, by means of three consecutive numbers, the degrees of freedom of the shoulder, elbow and hand articulations, respectively. The second one is by defining through a chain of letters each of the possible rotations of the articulations of the shoulder, elbow and hand. The AACMM used in the present work is a 7 DOF Platinum series FARO arm with a typical 2-2-3 configuration or a-b-c-d-e-f-g degrees of rotation (Fig. 1), with a nominal value of semirange of ± 0.030 mm obtained in a single-point articulation performance test of the arm manufacturer.

A continuous data capture method has been used for the self-centering probes, and discrete capture has been used for active and passive spherical probes. The continuous capture technique allows the massive capture of arm positions corresponding to several points of the workspace. To this end, a ball-bar gauge of 1.5 m long was placed in 7 positions within the workspace of the arm in order to cover the maximum number of possible AACMM positions, to subsequently extrapolate the results obtained throughout the volume. Fig. 2 and Table 1 show the considered positions for the ball-bar in a quadrant of the workspace. The ball-bar comprises a carbon fiber profile and 15 ceramic spheres of 22 mm in diameter, reaching calibrated distances between the centers with an uncertainty, in accordance with its calibration certificate, of (1+0.001L) μm, with L in mm. In this configuration, 4 spheres of the ball-bar in each of the 7 positions considered are probed, materializing 6 distances between their centers.

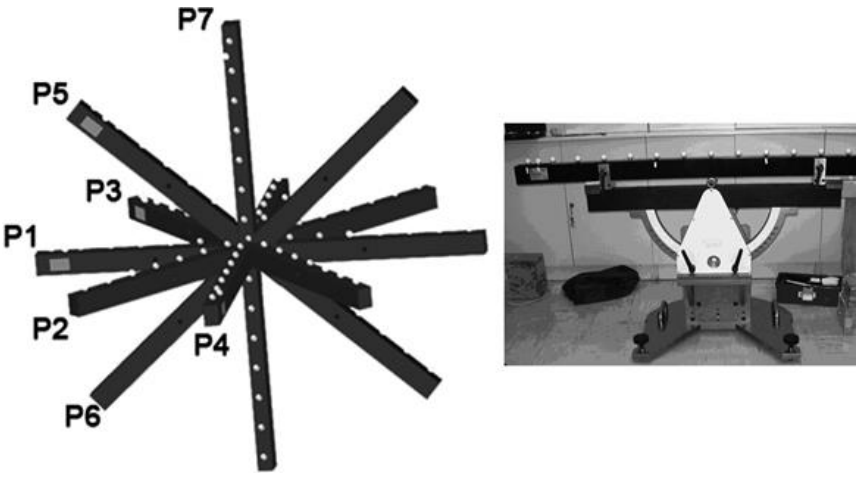

Fig. 2. Ball bar gauge test positions and support.

Table 1. List of ball bar gauge positions in quadrant 1.

Position No.	Quadrants	Tilt	Distance B1	Direction
1	C1-C2-C4	Horizontal	Medium	Tangential
2	C1-C4	Horizontal	Near	Tangential
3	C1-C2	Horizontal	Far	Tangential
4	C1	Horizontal	Near	Radial
5	C1-C2-C4	+45º	Medium	Tangential
6	C1-C2-C4	-45º	Medium	Tangential
7	C1	Vertical	Medium	Tangential

With passive and active spherical tip probes, around 25 points of the sphere surface have been captured in each measured sphere, while with the self-centering probes around 250 center points have been captured for each sphere (Fig. 3a). For these probes, besides characterizing the performance of the arm relative to error in distances, its capacity to repeat measurements of the same point is also tested.

Hence, automatic arm position capture software has been developed to probe each considered sphere of the ball-bar and to replicate the arm behavior in the single-point articulation performance test, but in this case, to evaluate its repeatability. The rotation angle values of the arm joints for each position, reached in the continuous probing of each sphere, are stored to obtain the coordinates of the measured point with respect to the global reference system for any set of parameters considered. In this way, with the self-centering probes in contact with the sphere, it is possible to capture the maximum possible number of arm positions, thus covering a large number of arm configurations for each sphere considered. The centering of the probe direction with regards to the sphere center is ensured with the self-centering probes, making this direction cross it (Fig. 3b) for any orientation of the probe. Thus, it is possible to define in this case a probe with zero probe sphere radius and with a distance of 22 mm from the position of the housing to the center of the probed sphere, allowing direct probing of the sphere center when the three spheres or planes of the probes and the sphere of the gauge are in contact. The details of the design, kinematic modeling and calibration of the self-centering probes is described in [1].

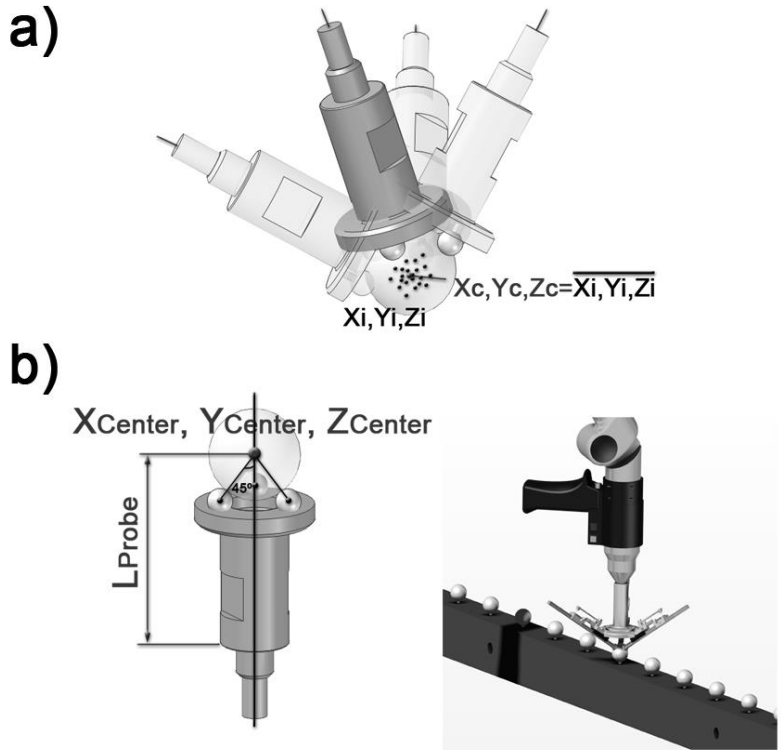

Fig. 3. a) Center points considered for distance error with self-centering probes.
b) Probing the center of a sphere with passive and active self-centering probes.

4. Test and results

In the configuration presented for both groups of probes, results of distance errors between centers have been obtained for each of the 6 distances materialized in each of the 7 ball-bar positions.

4.1. Spherical tip probes

In the case of passive and active spherical probes, the centers of the spheres were obtained by means of the least squares method, using the captured surface points. This also allowed us to obtain both the distance from each probed point to the surface of the sphere and the standard deviation of this distance. In Fig. 4 the graph shows the error in distance between the centers of the ball-bar spheres obtained with the active spherical probe against the error in distance between the centers obtained with the passive spherical probe, relative to the distances calculated with the ball-bar. With regard to the error in distance, we can observe that the error made with the active probe is slightly smaller than that made with the passive probe, except in positions 5 and 6. However, it is important to mention that the errors are almost equal in all positions. Moreover, Fig. 4 shows that most of the final error obtained with the AACMM in the probing of the spheres is due to the measuring instrument itself with a very low influence of the probing system chosen in each case. The fact that we get almost the same error values in the same positions of the ball-bar with different probing systems strongly suggests that the error map shown in this figure is mainly associated with inadequate values of the kinematic model parameters, which leads to similar errors in the same positions of the measured sphere. On the other hand, it is noteworthy that the expected benefit a priori derived from the use of active probes is not associated with a lesser influence of the probing force, but simply with a more comfortable capture process. This makes the cost of the active probing system unjustifiable, compared to the traditional passive probing systems.

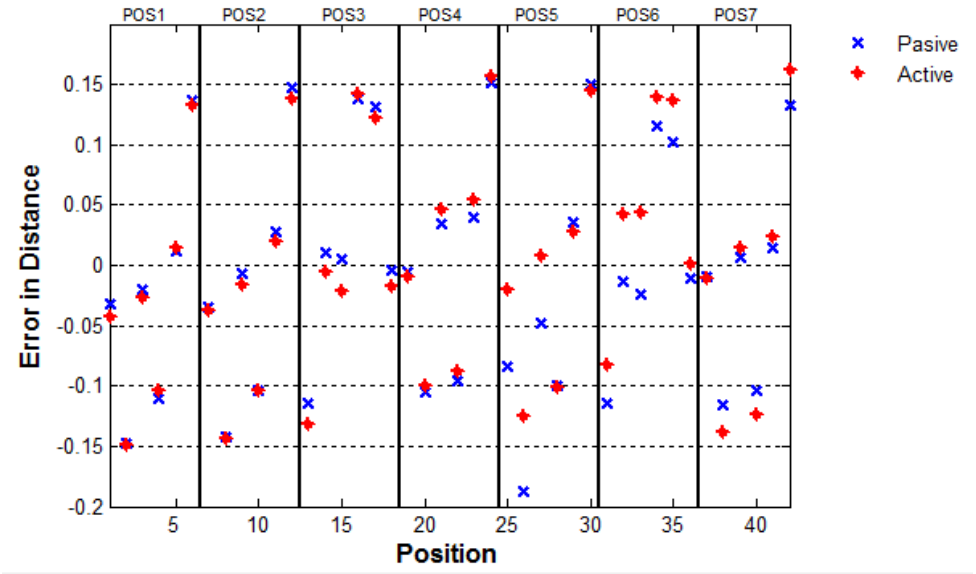

Fig. 4. Distance errors of the measured centers.

Fig. 5 shows the difference between the distance errors of active spherical probe and those of the passive spherical probe in all 42 positions that were used. When a positive difference is

obtained, the active spherical probe error is smaller and thus better than the active spherical probe, and vice versa when the difference is negative.

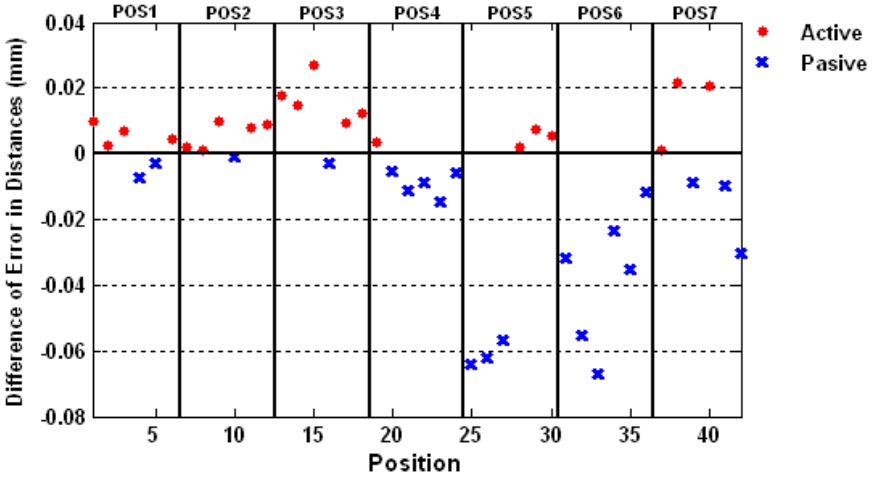

Fig. 5. Difference of distance error between active and passive probe.

4.2. Self-centering probes

In the case of the self-centering probes, the mean point of all the captured data for each sphere was considered as the center of the sphere probed (Fig. 3a). Measured distances for each sphere in the 7 different positions were compared with the distances obtained with the ball bar gauge thus obtaining the error in distance (Fig. 6), as well as the differences between the distance errors of the active spherical probe and the passive spherical probe in all 42 positions that were considered (Fig. 7).

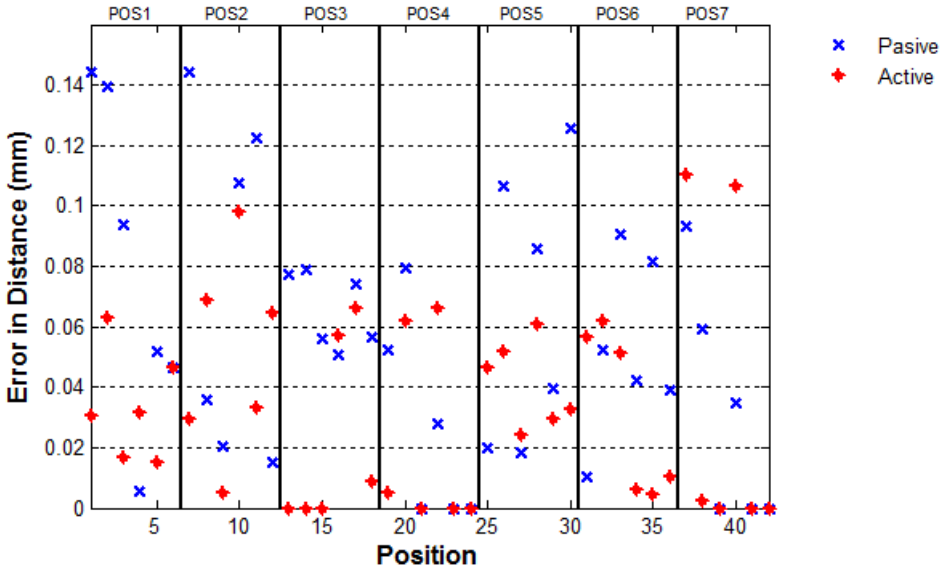

Fig. 6. Error in distance of the measured centers.

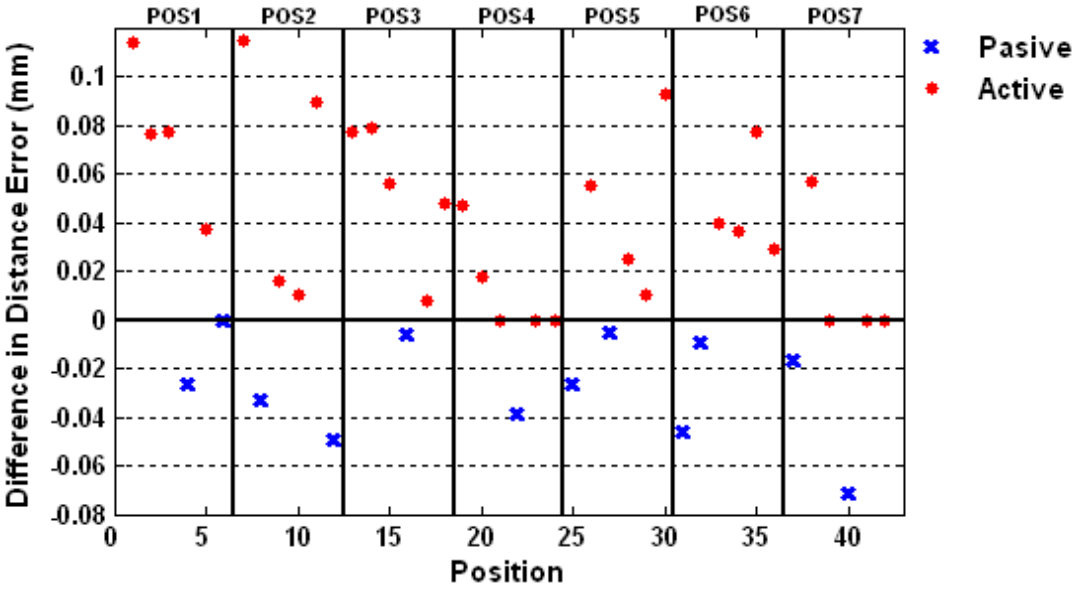

Fig. 7. Difference of distance error between active and passive probe.

A positive difference represents a smaller error in the active spherical probe and in that case this probe is considered to be better than the passive one. In the case of positions 3, 4 and 7, three spheres were not measured with the self-centering active probe (sphere 1 in position 3 and sphere 14 in positions 4 and 7)-because the arm was unable to properly reach these extreme positions with the active spherical probe mounted, so a value of zero was assigned in the graphs. From Fig. 6, it can be observed that on average, the error made by the self-centering active probe was less than the one corresponding to the self-centering passive probe; the errors obtained with the active probe, when greater than those corresponding to the passive probe, can be associated to the AACMM as it approaches its workspace frontier. The three-dimensional distances between spheres were obtained calculating the Euclidean distance $D_{i_{jk}}$ between the mean centers calculated for each sphere, where $D_{i_{jk}}$ represents the distance from sphere *j* to sphere *k* of ball-bar position *i*. If $D_{0\,jk}$ is defined as the nominal distance between spheres *j* and *k* obtained from the ball-bar calibration table, it is possible to calculate the error in distance between spheres *j* and *k* in location *i* as follows:

$$E_{i_{jk}} = \left| D_{i_{jk}} - D_{0ik} \right|. \tag{1}$$

The repeatability error values for all measured points are shown in Fig. 8a and 8b, for the self-centering active probe and self-centering passive probe respectively.

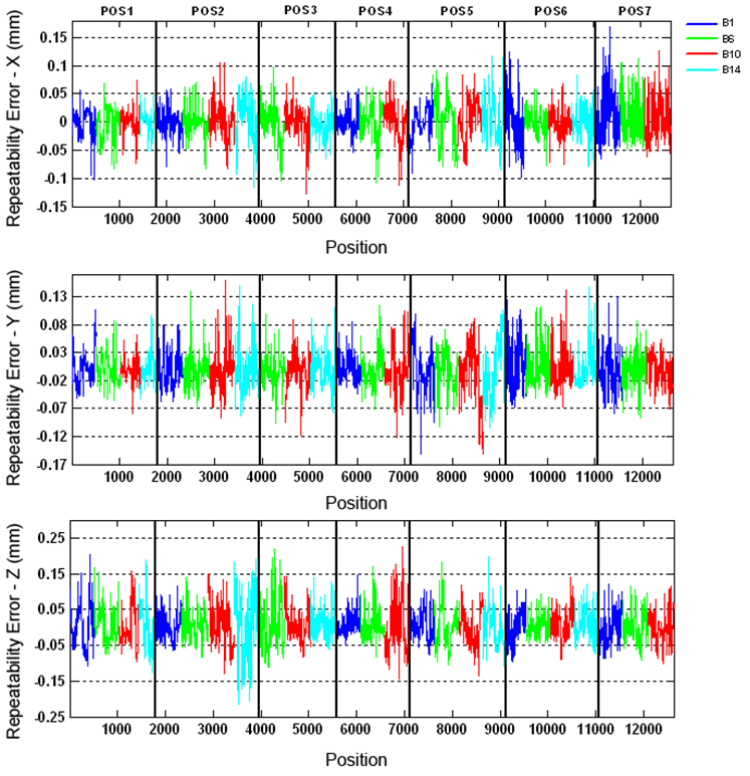

Fig. 8a. Point repeatability errors for the 7 AACMM positions using the active self-centering probe.

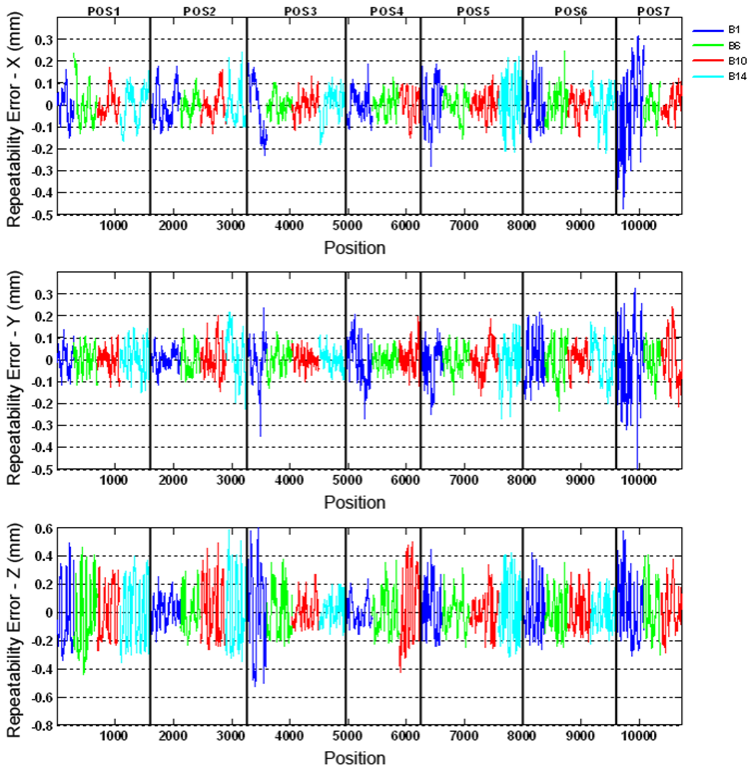

Fig. 8b. Point repeatability errors for the 7 AACMM positions using the passive self-centering probe.

These values represent the errors made in *X*, *Y* and *Z* coordinates of each one of the approximately 10000 points obtained, corresponding to the 7 positions of the ball-bar gauge with regards to the mean obtained for each sphere. The repeatability error value for each coordinate as a function of AACMM joint rotation angles is given by:

$$\begin{aligned} \varepsilon_{Xijk}(\theta_1,\theta_2,\theta_3,\theta_4,\theta_5,\theta_6) &= \bar{X}_{ij} - X_{ij} \\ \varepsilon_{Yijk}(\theta_1,\theta_2,\theta_3,\theta_4,\theta_5,\theta_6) &= \bar{Y}_{ij} - Y_{ij} \\ \varepsilon_{Zijk}(\theta_1,\theta_2,\theta_3,\theta_4,\theta_5,\theta_6) &= \bar{Z}_{ij} - Z_{ij} \end{aligned} \quad . \tag{2}$$

It can be observed that the error made by the self-centering active probe is much smaller than the error made by the self-centering passive probe and that in both graphs the error shows an increment in the *z* coordinate. This behavior in the *z* coordinate could be explained by the fact that, unlike what happens in the *x* and *y* coordinates, there is no self-compensation effect in the ball-bar deformation due to the probing force in this coordinate. Figure 9 shows the magnitude of the error vectors in the direction of the probing forces of every measurement on the sphere and the resultant of these vectors. As expected, the direction of the resultant vector (which is multiplied by a module 5 and in red) is downwards which as mentioned before is caused by lack of the self-compensation effect in the z coordinate.

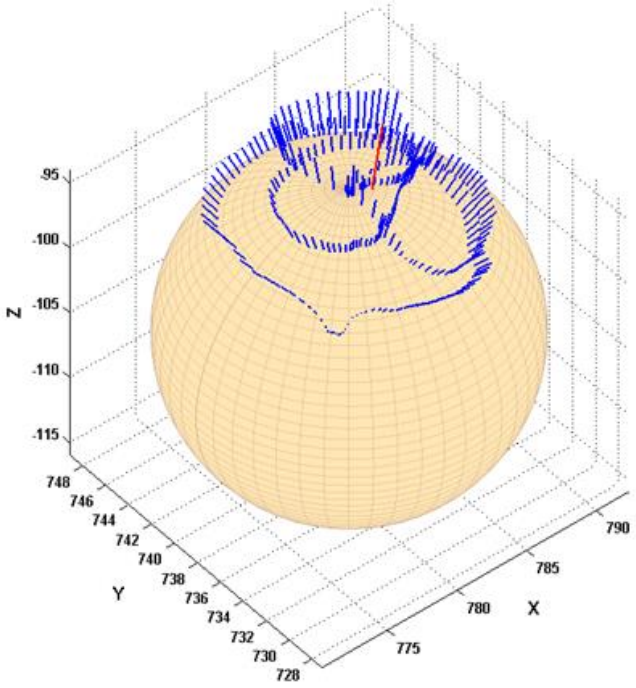

Fig. 9. Direction and magnitude of error vectors and resultant vector.

In Fig. 10, the standard deviation corresponding to the 7 different positions in *x*, *y* and *z* for both types of probes is shown. As expected, the standard deviation in the self-centering active probe is smaller than that of the one obtained with the self-centering passive probe, except as mentioned earlier, in the positions were spheres were not measured and a value of zero was assigned in the graph.

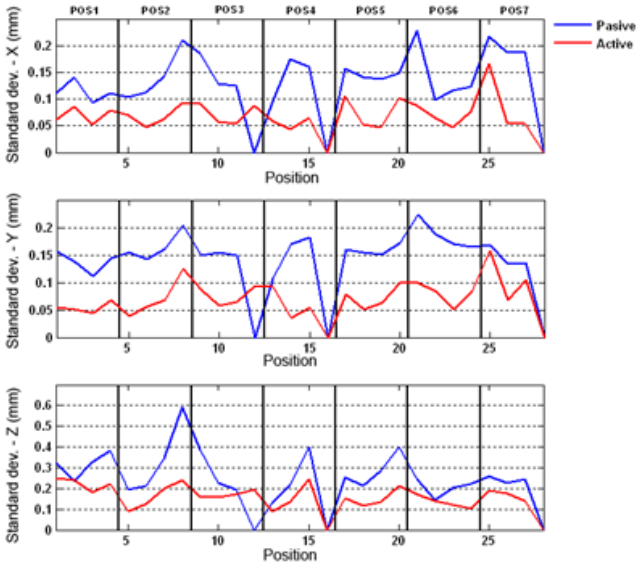

Fig. 10. Standard deviation of the sphere centers.

Another way of illustrating the influence of the probing direction over the probing error is by expressing the error magnitude in terms of the probed point reference system. Fig. 11a shows the reference system linked to the last articulation of the kinematic chain of the arm. By translating this reference system to the probed point as shown in Fig. 11b, we can express the error magnitude in terms of the probed point reference system. This is done for each of the probed points on the sphere.

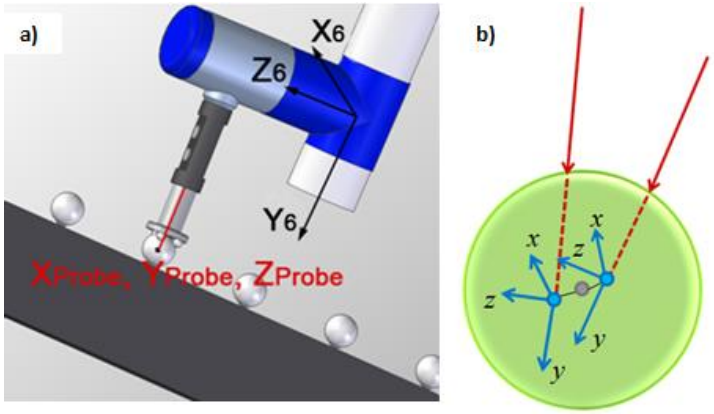

Fig. 11. a) Reference system linked to the last articulation of the AACMM,
b) magnitude error vector expressed in probed point reference system.

Figure 12 shows the values of the *X*, *Y* and *Z* coordinates expressed in the probed point's reference system for all the 10000 points obtained, corresponding to the 7 positions of the ball-bar with respect to the mean obtained for each sphere using the self-centering passive probe. As expected, since the probing direction is similar to the *Y* coordinate of the AACMM last articulation, the values in the *Y* coordinate are greater than those in the *X* and *Z* coordinates. This can be attributable to the probing force exerted by the operator over the measuring arm.

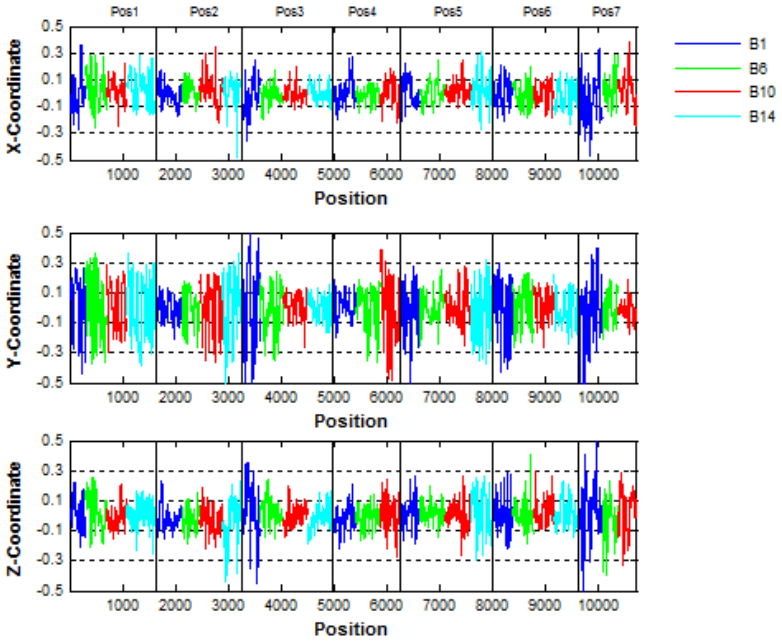

Fig. 12. *X*, *Y* and *Z* values (mm) expressed in probed points reference system.

For example, the values of the six articulations of the arm in position 1, when the maximum error exceeds .4 mm, are saved and shown in Fig. 13. This is done by precisely knowing the maximum and minimum values of the articulations throughout the tests and then obtaining those articulation values when the error is greater than .4mm. In the present graph, the range for each articulation in the measuring process is represented by a horizontal line of the same colour of the sphere being measured. This value was determined by calculating the mean and one sigma of the standard deviation of the values of Fig. 12 ($\mu \pm 1\sigma$). Moreover, Table 2 shows the percentage range of angle values for any combination of angles that result in an error greater than .4mm. This way, we can analyze the distribution of the angles that result in an error and observe if there is any pattern in any combination of articulation values that correspond to an error greater than .4 mm. In this particular analysis, no pattern could be observed, so most of the probing error could be explained by the probing force.

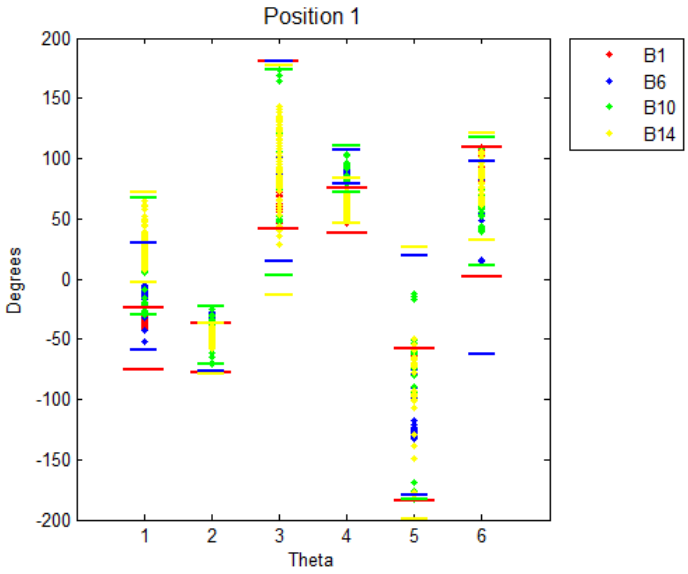

Fig. 13. Combination of articulation angles of an AACMM where the maximum error exceeds 4 mm for position 1 of the calibration ball bar gauge.

Table 2. Percentage range for any combination of angle values that result in errors greater than .4mm.

Sphere	Articulations					
	1	2	3	4	5	6
B1	65.44 - 91.16	57.31 - 91.07	3.58 - 24.32	21.08 - 69.15	85.44 - 97.69	47.45 - 100
B6	8.24 - 61.42	72.66 - 91.85	35.09 - 69.70	3.74 - 60.90	23.39 - 58.57	48.56 - 93.32
B10	0 - 70.44	.069 - 95.83	26.05 - 100	17.68 - 83.02	0 - 81.34	26.18 - 91.30
B14	13.88 - 91.70	50.41 - 95.79	22.48 - 82.37	4.14 - 71.10	9.07 - 66.68	33.19 - 83.42

4. Conclusions

In this work, a comparison between four different probing systems applied to capturing data for parameter identification and verification of an AACMM is presented. Besides the probing systems traditionally used in the verification of an AACMM, self-centering probing systems with kinematic coupling configuration and self-center active probing systems have also been used for the same purpose. Such probing systems are very suitable for use in verification procedures and capture of data for parameter identification, because they drastically reduce the capture time and the required number of positions of the gauge used as compared to the usual standard and manufacturer methods. These systems are also very suitable for their capacity of capturing multiple positions of the AACMM for a single gauge position, so that the accuracy results obtained after a procedure of identification or verification are more generalizable than those obtained with the traditional probing systems.

The effect of auto compensation of the gauge deformation has been shown by properly defining the trajectories of capture or the direction of probing during the process of capturing data. Moreover, it has been demonstrated that the smallest influence of the probing force is obtained in the case of the self-centering active probe. In addition, an analysis of the influence of the probing force over the final error was done by means of the error's vector decomposition and by expressing this decomposition in the probed point reference system. Furthermore, as mentioned above, since the final error depends on the combined influence of all joints, with the presented analysis it is possible to determine on the one hand the influence over the error of the probing itself and the relationship of that error with the AACMM pose if there exists one, thus making possible to identify sets of joint angle values that lead to greater probing errors. Finally, the adequacy of the self-center active probes over self-center passive probes and spherical tip probes for tasks such as capturing data for verification and identification of kinematics parameters has been demonstrated when no configuration or application restrictions are imposed.

Acknowledgements

The support of Consejo Nacional de Ciencia y Tecnología (Concayt) and Dirección

General de Educación Superior Tecnológica (DGEST) is deeply acknowledged by the first and second authors. This work was supported by the DICON Innpacto Project (IPT-2011-1191-020000), Development of new advanced dimensional control systems in manufacturing processes of high-impact sectors. A preliminary version of the results was presented at the XIX IMEKO World Congress Fundamental and Applied Metrology, "Performance evaluation of probing systems in data capture for kinematic parameter

identification and verification of articulated arm coordinate measuring machines", Lisbon, Portugal, 2009.

References

[1] Santolaria, J., Brau, A., Velázquez, J., Aguilar, J. J. (2010). A self-centering active probing technique for kinematic parameter identification and verification of articulated arm coordinate measuring machines. *Meas. Sci. Technol.*, 21(5), 055101.

[2] Gatti, G., Danieli, G. (2008). A practical approach to compensate for geometric errors in measuring arms: application to a six-degree-of-freedom kinematic structure. *Meas. Sci. Technol.*, 19(1), 015107.

[3] Kovac, I., Frank, A. (2001). Testing and calibration of coordinate measuring arms. *Precis. Eng.*, 25(2), 90–99.

[4] Denavit, J., Hartenberg, R. S. (1955). A kinematic notation for lower-pair mechanisms based on matrices. *Trans ASME J. Appl. Mech*, 23, 215–221.

[5] Hayati, S., Mirmirani, M. (1985). Improving the absolute positioning accuracy of robot manipulators. *J. Robot. Syst.*, 2(4), 397–413.

[6] Elatta, A. Y., Gen, Pei L., Zhi Liang, F., Daoyuan, Y., Fei, L. (2004). An Overview of Robot Calibration. *Inf. Technol. J.*, 3(1), 74–78.

[7] Santolaria, J., Aguilar, J., Yague, J., Pastor, J. (2008). Kinematic Parameter Estimation Technique for Calibration and Repeatability Improvement of Articulated Arm Coordinate Measuring Machines. *Precis. Eng.*, 32(4), 251–268.

[8] Ratajczyk, E., Rak, M., Kowaluk, T. (2012). The influence of method of point collection on results with the use of a measuring arm. *Metrol. Meas. Syst.*, XIX(3), 541–552.

[9] Everett, L., Driels, M., Mooring, B. (1987). Kinematic modelling for robot calibration. *Proceedings. 1987 IEEE International Conference on Robotics and Automation, Institute of Electrical and Electronics Engineers*, 183–189.

[10] Huang, C., Xie, C., Zhang, T. (2008). Determination of optimal measurement configurations for robot calibration based on a hybrid optimal method. *2008 International Conference on Information and Automation*, 789–793.

[11] Roth, Z., Mooring, B., Ravani, B. (1987). An overview of robot calibration. *IEEE J. Robot. Autom.*, 3(5), 377–385.

[12] Hamana, H., Tominaga, M., Ozaki, M., Furutani, R. (2010). Calibration of Articulated Arm Coordinate Measuring Machine Considering Measuring Posture. *10th Internanational Symposium on Measurement and Quality Control*, 5–8.

[13] Piratelli-filho, A., Henrique, F., Fernandes, T., Valdés, R. (2012). Application of Virtual Spheres Plate for AACMMs evaluation. *Precis. Eng.*, 36(2), 349–355.

[14] Zheng, D., Du, C., Hu, Y. (2012). Research on optimal measurement area of flexible coordinate measuring machines. *Measurement*, 45(3), 250–254.

[15] Kupiec, M. (2012). Coordianate Measurment Systems Cmm and Cma – Characteristc and Methods of Their Accuracy Evaluation. *Adv. Sci. Technol. – Res. J.*, 6(16), 17–23.

[16] Sładek, J., Ostrowska, K., Gąska, A. (2013). Modeling and Identification of Errors of Coordinate Measuring Arms with the Use Of A Metrological Model. *Measurement*, 46, 667–679.

[17] Li, X. H., Chen, B., Qiu, Z. R. (2012). The Calibration and Error Compensation Techniques for an Articulated Arm CMM with two Parallel Rotational Axes. *Measurement*, 46(1), 603-609.

[18] Alici, G., Shirinzadeh, B. (2005). A systematic technique to estimate positioning errors for robot accuracy improvement using laser interferometry based sensing. *Mech. Mach. Theory*, 40(8), 879–906.

[19] Gong, C., Yuan, J., Ni, J. (2000). Nongeometric error identification and compensation for robotic system by inverse calibration. *Int. J. Mach. Tools Manuf.*, 40(14), 2119–2137.

[20] Ali, S. H. R. (2010). Probing System Characteristics in Coordinate Metrology. *Meas. Sci. Rev.*, 10(4), 120–129.

[21] Weckenmann, A., Estler, T., Peggs, G., McMurtry, D. (2004). Probing Systems in Dimensional Metrology. *CIRP Ann. - Manuf. Technol.*, 53(2), 657–684.

[22] ASME B89.4.22:, (2004). *Performance Evaluation of Articulated Arm Coordinate Measuring Machines*.

[23] Trapet, E., Aguilar Martin, J., Yague, J., Spaan, H., Zeleny, V. (2006). Self-centering probes with parallel kinematics to verify machine-tools. *Precis. Eng.*, 30(2), 165–179.